applied sciences

MDPI

Article

Comprehensive Evaluations of NLOS and Linearization Errors on UWB Positioning

Yan Li, Zhouzheng Gao *, Qiaozhuang Xu and Cheng Yang

School of Land Science and Technology, China University of Geosciences Beijing, Beijing 100083, China; liyan0415@email.cugb.edu.cn (Y.L.); qiaozhuangxu@email.cugb.edu.cn (Q.X.); c.yang@connect.polyu.hk (C.Y.)
* Correspondence: zz.gao@cugb.edu.cn; Tel.: +86-186-2791-5172

Abstract: Currently, ultra-wide band (UWB) is adopted as a useful high-accuracy positioning technique in satellite-blocked areas. However, UWB's positioning performance would be limited significantly because of non-line of sight (NLOS) errors. Additionally, the truncation errors in these linearization-based adjustments such as least squares (LS) and extended Kalman filter (EKF) would also visibly degrade UWB positioning accuracy. To overcome the impacts of NLOS errors and truncation errors, this paper introduced a robust-theory-based particle filter (RPF) into UWB positioning. In such a method, the IGG-III model and PF were adopted to limit the impacts of NLOS errors and truncation errors, respectively, by introducing a weight inflation factor and particle group. For comparison, the Bancroft, LS, EKF, unscented Kalman filter (UKF), cubature Kalman filter (CKF), PF, and RPF were also presented. Here, the influences of truncation errors were analyzed by comparing the results based on LS and EKF with those calculated by UKF, CKF, and PF. The impacts of NLOS errors were evaluated by making a comparison between the results of PF and RPF. Results based on a set of simulated UWB data and a group of experiment UWB data demonstrated that the RPF can significantly avoid the positioning errors caused by both truncation errors and NLOS errors. In general, position improvements percentages of 57.2%, 52.7%, 39.6%, 38.2%, 26.6%, and 20.4% can be obtained by RPF compared to those calculated by Bancroft, LS, EKF, UKF, CKF, and PF, respectively. As a comparison, the truncation error would lead to about 8.1%, 10.1%, and 33.2% accuracy decrease in the north, east, and vertical directions on average. Such accuracy-decrease rates caused by NLOS were 6.1%, 5.2%, and 25%.

Keywords: ultra-wide band (UWB); non-line of sight (NLOS); truncation error; robust particle filter (RPF)

check for updates

Citation: Li, Y.; Gao, Z.; Xu, Q.; Yang, C. Comprehensive Evaluations of NLOS and Linearization Errors on UWB Positioning. *Appl. Sci.* **2023**, *13*, 6187. https://doi.org/10.3390/app13106187

Academic Editors: Sven Casteleyn, Aleksandr Ometov and Joaquín Torres-Sospedra

Received: 15 April 2023
Revised: 9 May 2023
Accepted: 16 May 2023
Published: 18 May 2023

1. Introduction

High accuracy requirement in indoor positioning applications is growing rapidly. Although global navigation satellite systems (GNSS, i.e., BDS and GPS) satisfy users' high-accuracy location service needs in open environments [1], it is difficult for GNSS to provide location services [2] in satellite signals blocked areas, such as indoor environments [3]. To this end, researchers studied indoor positioning methods based on infrared [4], ultrasonic [5], Bluetooth [6], Wi-Fi [7,8], and PDR [9,10]. These techniques have obvious weaknesses of low accuracy and short distance. For example, infrared light is easily blocked by walls during transmission, which leads to a short transmission distance [11]. Ultrasound is measured by echo signal resulting high accuracy position solution, but multi-path and non-line of sight (NLOS) will degrade the accuracy. Bluetooth technology is only available in small areas. In large-range areas, the signal stability is poor, resulting in low positioning accuracy [12]. Wi-Fi, with the advantages of low cost, wide signal source, and wide range, is supported by the location information of network nodes. However, it provides a low accuracy position and is easily affected by environments [13]. In addition, these indoor positioning techniques are mainly used in horizontal positioning, which cannot meet the urgent demand for high-precision indoor three-dimensional positioning.

In order to overcome these shortcomings existing in conventional indoor positioning methods, an indoor positioning method based on ultra-wideband (UWB) was proposed. Compared with the indoor positioning technologies mentioned above, UWB has the advantages of high interference resistance, low power consumption, and high range accuracy [14,15]. Additionally, UWB has a strong penetration ability under the situations such as in woods and stones, and these penetration errors can be corrected by modeling. However, UWB has a weak ability to penetrate water and metal [16]. Currently, UWB modes include Time of Arrival (TOA), Time of Flight (TOF), Difference of Time-Of-Arrival (TDOA), Angle of Arrival (AOA), Received Signal Strength Indication (RSSI) [17,18]. TOF is widely used in indoor applications because the tag does not need to be synchronization with the base station precisely [19,20].

However, while suffering complex indoor environments, indirect UWB signals will be received because of reflection, refraction, diffraction, or passing through walls [1]. Such indirect signals could increase transmission time and lead to NLOS ranging errors. NLOS errors result in a major impact on the UWB positioning accuracy. Additionally, since the relationship between the UWB range and the tag's position is nonlinear, it is necessary to linearize the observation function by Taylor expansion while using the traditional least squares (LS) and extended Kalman filter (EKF). Here, only the first-order item in Taylor expansion was adopted and the second-order and higher-order terms were abandoned. However, for the UWB ranging system, its maximum ranging distance was no more than hundreds of meters at present (https://www.nooploop.com/en/, accessed on 9 May 2023). Therefore, omitting higher-order terms in LS and EKF would introduce significant linearization errors, which could result in an accuracy degradation and even lead to a divergence in parameter estimation [21]. Therefore, reducing the impacts of NLOS errors and linearization errors on UWB positioning accuracy is an important issue for UWB-based indoor positioning technologies.

In recent years, many works were carried out on the effects of attenuated NLOS errors and linearization errors on the positioning accuracy of UWB. For the NLOS error, Guvenc et al. [22] introduced a novel weighted least squares (WLS) algorithm that used the LOS likelihood values. The improvements compared to the conventional LS were demonstrated firstly via Monte Carlo simulations. Then, it was verified by using TOA data, and the results showed that WLS was superior to LS in NLOS conditions. Li et al. [23] proposed a factor graph-based UWB positioning algorithm based on an improved Turkey robust kernel, which was verified via a set of NLOS UWB-TOA data. The experimental results proved that the UWB positioning algorithm based on the improved Turkey robust kernel outperformed the LS algorithm in NLOS environments. The corresponding positioning accuracy improvements on average were 20–30%. Dong et al. [24] proposed an improved robust adaptive cubature Kalman filter (IRACKF) algorithm. The autocorrelation covariance matrix-based robust algorithm was used to alleviate the impact of these NLOS errors polluted UWB data on the UWB positioning accuracy. The results based on both simulation and field experiments showed that IARCKF can reduce positioning errors by the percentages of 52.6%, 38.0%, 45.1%, and 25.3% compared with the solutions of CKF, robust cubature Kalman filter (RCKF), adaptive cubature Kalman filter (ACKF), and robust adaptive CKF (RACKF), respectively.

Fu et al. [25] adopted an adaptive unscented Kalman filter (UKF) filter in the UWB system. The experiment test presented its adaptive ability, and the positioning accuracy of UWB can be upgraded to 7 cm on average. Wu et al. [26] proposed the adaptive square root cubature Kalman filtering (ASRCKF) algorithm to solve the problem that the filtering accuracy decreases when the measurements are abnormal. It was verified by using TDOA/AOA combined data. The results showed that the RMSE of ASRCKF was slightly affected and the tag's position can converge to the real value rapidly. Otim et al. [14] developed a positioning system based on particle filter (PF). The results proved that about

75% and 82% reduction in the median position error in simulation and experiment tests with providing sub-meter level positioning accuracy.

Although the UWB positioning technique was studied, the influence of different parameter estimation methods on UWB positioning accuracy, and the impacts of linearization error and NLOS error on UWB 3D positioning accuracy were not analyzed comprehensively. Hence, we adopted a robust particle filter (RPF) to evaluate the effects of NLOS errors and linearization errors on the UWB positioning accuracy in both horizontal and vertical components based on the simulated and measured TOF UWB data. For comparison, the conventional methods including the Bancroft algorithm, LS, EKF, UKF, CKF, and PF were also analyzed. Compared to the existing works, the contributions of our work are that (1) we considered both NLOS errors and linearization errors in UWB 3D positioning, and provided the RPF to reduce their impacts on UWB positioning accuracy; and (2) we analyzed linearization errors by comparing the results based on LS and EKF with those based on UKF, CKF, and PF. The paper is arranged as: Section 2 introduces the relevant mathematical principles and the details of the proposed positioning algorithm, Section 3 introduces the experiments and results, which is followed by conclusions in Section 4.

2. Methods

TOF-UWB tag communicates with the base stations for ranging and exchanging timestamp information. The distance from the tag to each base station was d_i (i = 1, 2, . . . , N, N is the number of base stations), which can be expressed as [27]

$$\begin{cases} d_1^2 = (x - x_1)^2 + (y - y_1)^2 + (z - z_1)^2 \\ d_2^2 = (x - x_2)^2 + (y - y_2)^2 + (z - z_2)^2 \\ \vdots \\ d_N^2 = (x - x_N)^2 + (y - y_N)^2 + (z - z_N)^2 \end{cases} \tag{1}$$

where (x, y, z) and (x_i, y_i, z_i) are the coordinates of the tag and base station.

As shown in Equation (1), the relationship between UWB ranging distances and the tag's coordinates is nuclearization. Meanwhile, such a strict relationship would be destroyed while suffering NLOS errors or while using the linearized adjustment methods. Therefore, the traditional linearized adjustment methods named as least square and extended Kalman filter were first provided. Then, the robust particle filter was introduced in detail.

2.1. Least Square

While using LS, the tag coordinates $X = (\delta_x, \delta_y, \delta_z)$ can be computed as shown in (2) [28]

$$\boldsymbol{X} = (\boldsymbol{A}^{\mathrm{T}}\boldsymbol{A})^{-1}\boldsymbol{P}\boldsymbol{A}^{\mathrm{T}}\boldsymbol{b} \tag{2}$$

where $\begin{cases} x = \hat{x} + \delta_x \\ y = \hat{y} + \delta_y \\ z = \hat{z} + \delta_z \end{cases}$, $\boldsymbol{b} = \begin{bmatrix} d_1 - \hat{d}_1 \\ d_2 - \hat{d}_2 \\ \vdots \\ d_N - \hat{d}_N \end{bmatrix}$, $\boldsymbol{A} = \begin{bmatrix} \frac{\hat{x}-x_1}{\hat{d}_1} & \frac{\hat{y}-y_1}{\hat{d}_1} & \frac{\hat{z}-z_1}{\hat{d}_1} \\ \frac{\hat{x}-x_2}{\hat{d}_2} & \frac{\hat{y}-y_2}{\hat{d}_2} & \frac{\hat{z}-z_2}{\hat{d}_2} \\ \vdots & \vdots & \vdots \\ \frac{\hat{x}-x_N}{\hat{d}_N} & \frac{\hat{y}-y_N}{\hat{d}_N} & \frac{\hat{z}-z_N}{\hat{d}_N} \end{bmatrix}$, and $\boldsymbol{P}$ is the priori weight matrix.

2.2. Extended Kalman Filter

The standard Kalman filter (KF) applies to linear systems [29]. When the state transition function and/or observation function are nonlinear transformations, the standard KF cannot be used. The EKF linearizes the nonlinear system locally and can be applied to the weak nonlinear system [30]. The core idea is to apply the Taylor expansion to the nonlinear function at the filtering value and ignore the quadratic and above terms [31]. A typical nonlinear model can be expressed as [32]

$$\begin{cases} \boldsymbol{X}_k = \boldsymbol{f}(\boldsymbol{X}_{k-1}) + \boldsymbol{w}_k \\ \boldsymbol{Z}_k = \boldsymbol{h}(\boldsymbol{X}_K) + \boldsymbol{v}_k \end{cases} \tag{3}$$

where $\boldsymbol{X}_k$ is the state vector; $\boldsymbol{f}(\boldsymbol{X}_{k-1})$ is the system nonlinear function; $\boldsymbol{Z}_k$ is the measured value at time k; $\boldsymbol{w}_k$ and $\boldsymbol{v}_k$ represent process noise and measurement noise, respectively; $\boldsymbol{h}(\boldsymbol{X}_k)$ represents the nonlinear observation function [33].

The normal speed model is used as the equation of state. The state vector consists of position ($\boldsymbol{p}$) and velocity ($\dot{\boldsymbol{p}}$)

$$\boldsymbol{X}_k = \underbrace{\begin{pmatrix} \boldsymbol{I} & \boldsymbol{I}\Delta t \\ \boldsymbol{0} & \boldsymbol{I} \end{pmatrix}}_{\boldsymbol{F}} \underbrace{\begin{pmatrix} \boldsymbol{p} \\ \dot{\boldsymbol{p}} \end{pmatrix}}_{\boldsymbol{x}_{k-1}} + \underbrace{\begin{pmatrix} \boldsymbol{0} \\ \boldsymbol{w}_{\dot{\boldsymbol{p}}} \end{pmatrix}}_{\boldsymbol{w}_k} \tag{4}$$

where $\boldsymbol{F}$ represents the state transfer matrix; $\boldsymbol{I}$ is the unit vector; $\boldsymbol{w}_{\dot{\boldsymbol{p}}}$ is the velocity noise.

The EKF algorithm consists of two parts, with (1) Time-update [34]

$$\hat{\boldsymbol{X}}_{k+1|k} = \boldsymbol{F}\hat{\boldsymbol{X}}_k + \boldsymbol{w}_k \tag{5}$$

$$\boldsymbol{P}_{k+1|k} = \boldsymbol{F}\boldsymbol{P}_k\boldsymbol{F}^{\mathrm{T}} + \boldsymbol{Q} \tag{6}$$

and (2) Measurement-update [35]

$$\boldsymbol{K}_{k+1} = \boldsymbol{P}_{k+1|k}\boldsymbol{H}_{k+1}^{T}\left(\boldsymbol{H}_{k+1}\boldsymbol{P}_{k+1|k}\boldsymbol{H}_{k+1}^{\mathrm{T}} + \boldsymbol{R}\right)^{-1} \tag{7}$$

$$\hat{\boldsymbol{X}}_{k+1} = \hat{\boldsymbol{X}}_{k+1|k} + \boldsymbol{K}_{k+1}(\boldsymbol{Z}_{k+1} - \boldsymbol{h}(\hat{\boldsymbol{X}}_{k+1|k})) \tag{8}$$

$$\boldsymbol{P}_{k+1} = \boldsymbol{P}_{k+1|k} - \boldsymbol{K}_{k+1}\boldsymbol{H}_{k+1}\boldsymbol{P}_{k+1|k} \tag{9}$$

where $\boldsymbol{Q}$ is the system noise covariance matrix; $\boldsymbol{R}$ is the measurement noise covariance matrix; $\boldsymbol{H}_{k+1}$ is the Jacobian matrix.

2.3. Robust Particle Filter

The core idea of the PF algorithm is to select a group of particles randomly to replace the posterior probability distribution of the current system state. When the system is nonlinear, this algorithm has better filtering performance and the ability to deal with the influence of non-Gaussian noise compared with other algorithms. Therefore, it is widely used in the positioning system [36].

The recursive formula of PF is as follows:

(1) Setting the initial value X_0;
(2) Particle initialization: Sampling particle ($\boldsymbol{x}_{i,0}$, i = 1, 2, . . . , m) is generated from the prior probability distribution $p(X_0)$;
(3) Predictive step

$$\boldsymbol{x}_{i,1} = \boldsymbol{F}\boldsymbol{x}_{i,0} + \boldsymbol{q}_i \tag{10}$$

where $\boldsymbol{q}_i$ is random vector obeying $\boldsymbol{N}$ (0, $\boldsymbol{Q}$);
(4) Update step

The observation noise is assumed to obey the Gaussian distribution with the variance $\boldsymbol{R}$, and then, the corresponding weight $\boldsymbol{w}_{i,1}$ of the particle $\boldsymbol{x}_{i,1}$ is calculated [37] by

$$\boldsymbol{w}_{i,1} = f_R[\boldsymbol{Z}_1 - h(\boldsymbol{x}_{i,1})]\boldsymbol{w}_{i,0}\boldsymbol{\lambda}_i = \frac{1}{\sqrt{2\pi\boldsymbol{R}}}e^{-\frac{[\boldsymbol{Z}_1 - h(\boldsymbol{x}_{i,1})]^2}{2\boldsymbol{R}}}\boldsymbol{w}_{i,0} \tag{11}$$

(5) Normalization of weights

$$\boldsymbol{w}_{i,1} = \frac{\boldsymbol{w}_{i,1}}{\sum \boldsymbol{w}_{i,1}} \tag{12}$$

(6) Particle resampling

There is a problem of particle degradation in the application of PF algorithm. That is the weights of most particles change to very small, while only a few particles hold very large weights after several iterations. These particles with very small weights will be replaced by new particles.

The independent random samples $\left\{\boldsymbol{u}_{n,1}\right\}_{n=1}^{m}$ selected from uniformly distributed are compared with the cumulative sum of normalized weights to select particles [38]. From the point of view of selecting particles, in the nth (n = 1, 2, . . . , m) selection, if there is a particle $\boldsymbol{x}_{i,1}$ that satisfies the conditions of (13) in the cumulative sum of weight values, the selected sample particles will be selected.

$$\sum_{j=1}^{i-1} w_{j,1} < u_{n,1} < \sum_{j=1}^{i} w_{j,1}, j = 1, 2, \ldots, i \tag{13}$$

Finally, the new particle set $\{x_{i,1}\}_{i=1}^{m}$ after resampling can be obtained.

(7) Optimal state estimate

From steps (1)~(6), particle $\boldsymbol{x}_{i,1}$ at k = 1 and the corresponding weights $\boldsymbol{w}_{i,1}$ are obtained. Then, the state estimate for k = 1 can be calculated by

$$\hat{\boldsymbol{X}}_1 = \sum_{i=1}^{m} \boldsymbol{w}_{i,1}\boldsymbol{x}_{i,1} \tag{14}$$

In the above steps, the optimal estimated value is obtained by PF, and it then progresses to the next iteration. Particle is introduced into the state transition equation to obtain a particle set. Then, weight and weight normalization are obtained by step (4) to obtain the optimal system state estimators for epoch k (=1, 2, 3, . . .).

When observations contain only accidental errors, the state can be approximated by a large number of particles. However, the UWB positioning accuracy will be polluted seriously while there are NLOS signals. In order to reduce the influence of abnormal observation, the IGG-III model is introduced into PF. The weight of the particle is changed when the observed value contains NLOS by

$$\bar{\boldsymbol{w}}_{i,1} = \boldsymbol{w}_{i,1}\boldsymbol{\lambda}_i \tag{15}$$

where $\boldsymbol{\lambda}_i$ is a weight inflation factor, which can be expressed as

$$\boldsymbol{\lambda}_i = \begin{cases} 1 & \left|\widetilde{\boldsymbol{V}}_i\right| \leq k_0 \\ \frac{k_0}{\left|\widetilde{\boldsymbol{V}}_i\right|}\left(\frac{k_1 - \left|\widetilde{\boldsymbol{V}}_i\right|}{k_1 - k_0}\right)^2 & k_0 < \left|\widetilde{\boldsymbol{V}}_i\right| \leq k_1 \\ 0 & \left|\widetilde{\boldsymbol{V}}_i\right| > k_1 \end{cases} \tag{16}$$

where $\widetilde{\boldsymbol{V}}_i$ is the standardized residual; k_0 and k_1 are constants, with k_0 = 1.0∼1.5, k_1 = 2.5∼8.0 [39].

Table 1 summarizes the advantages and disadvantages of the existing adjustments that can be used in UWB positioning.

Table 1. Advantages and disadvantages of algorithms.

Algorithm	Advantages	Disadvantages
Bancroft	This algorithm does not need to iterate the direct solution method with algebraic analytic properties and the solution speed is fast [40].	This algorithm cannot achieve the optimal solution in terms of statistical characteristics.
LS	The optimal matching method between data is found by finding the sum of minimum error squares [41].	It does not have error resistance, a small amount of gross error can cause unreliable parameter estimation, and the number of iterations and position accuracy are affected by the initial value.
EKF	The EKF linearizes the nonlinear system locally and can be applied to the weak nonlinear system.	When linearizing the nonlinear equation, EKF retains only one term coefficient, and the truncation error caused by discarding the higher-order term will have a significant impact on positioning accuracy [21].
UKF	The UKF approximates the posterior probability density function of the nonlinear system through UT transformation, and computes the mean value and covariance of the state vector, avoiding the linearized truncation error [42].	UKF has poor robustness in the case of system state mutation, and its accuracy is easily affected.
CKF	CKF algorithm uses spherical radial volume criterion to approximate the state posterior distribution of optimal estimation. CKF can not only overcome the shortcomings of UKF in high and strong nonlinear state estimation. However, it also has higher filtering accuracy [25].	The standard CKF requires Cholesky decomposition of the covariance of the posterior state when constructing volume points. This requires that the covariance of the transfer is a non-negative definite matrix, and the decomposition operation not only consumes time, but also reduces the stability of the increment algorithm [43].
PF	The core idea of the PF algorithm is to randomly select a group of particles to replace the posterior probability distribution of the current system state [44]. When the system is in a nonlinear environment, compared with other algorithms, this algorithm has better filtering performance and the ability to deal with the influence of non-Gaussian noise, so it is more and more widely used in the positioning system.	When the target state changes or bad measurement occurs, the tracking performance of the PF algorithm will decrease. The calculation is large and the calculation time is long.
RPF	The influence of anomaly observation is weakened and the accuracy of parameter estimation and the reliability of filtering are improved [45].	The calculation is large and the calculation time is long.

Based on the above models, the proposed UWB algorithm can be simply presented in Figure 1. Firstly, use eight LinkTrack P base stations (https://www.nooploop.com/en/. accessed on 9 May 2023) to collect the distance between each base station and the tag. Then, seven algorithms, namely Bancroft, LS, EKF, UKF, CKF, PF, and RPF, were used to calculate the positions of the tag. Finally, the impacts of NLOS errors and linearization errors on the UWB positioning accuracy were analyzed using indicators such as RMSE, CDF curve, and running time of different algorithms.

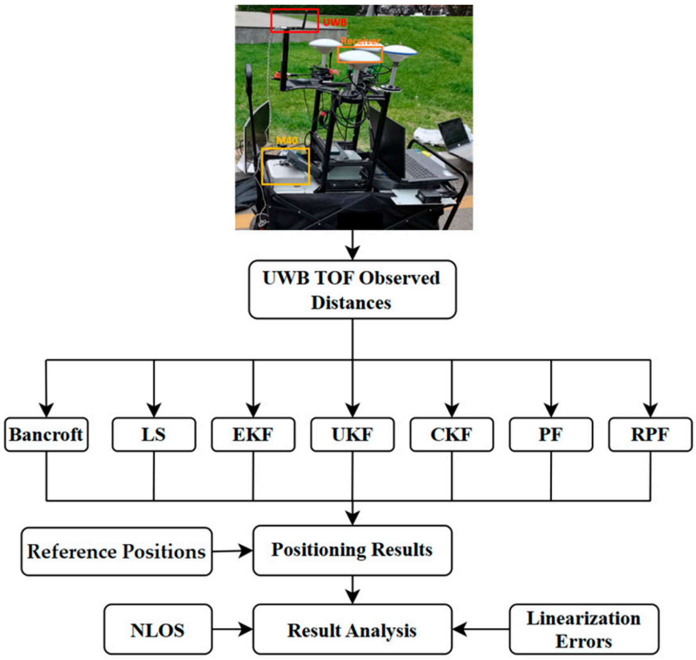

Figure 1. Algorithm structure of UWB positioning.

3. Tests and Evaluation

In order to investigate the impacts of NLOS and truncation errors on UWB positioning, the practical UWB data collected by LinkTrack P (Table 2) and the corresponding simulated UWB data were analyzed. These UWB data, ranging the distance between the tag and different base stations, were synchronized by using the NAssistant software (https://www.nooploop.com/en/download/, accessed on 9 May 2023) provided by Nooploop Company. Since the Nooploop Company increases UWB's transmission power, it makes the maximum UWB ranging distances up to 500 m. Meanwhile, a GNSS/INS-integrated navigation system and a Leica electronic total station were also adopted to provide the reference position solutions and the coordinates of UWB base stations. Here, the reference positions were calculated by the tightly coupled integration of real-time kinematic (RTK) and INS. Then, the position differences between the reference positions and these positions calculated by Bancroft, LS, EKF, UKF, CKF, PF, and RPF will be projected into the local leveling frame (North-East-Down), and the corresponding statics in terms of maximum values, averages, and standard deviation will be used to present the positioning accuracy of UWB. Here, the position errors in the north and east directions were to present the horizontal positioning accuracy, and the position errors in the down component were to illustrate the vertical positioning accuracy. Figure 2a,b show, respectively, the experimental environment and the detailed trajectory of the experiments. Figure 2c shows the distribution of eight UWB base stations. During the practical data collection, NLOS errors were generated by arranging people passing different base stations at different times. In the simulation experiment, the desired tag's position was set as the center of these eight base stations. Then, the UWB distances between the tag and eight base stations simulated by only adding the Gaussian distribution white noises with a mean value of 0.0 m and standard deviation of 0.3 m, and no NLOS errors were added.

(**a**)

(**b**)

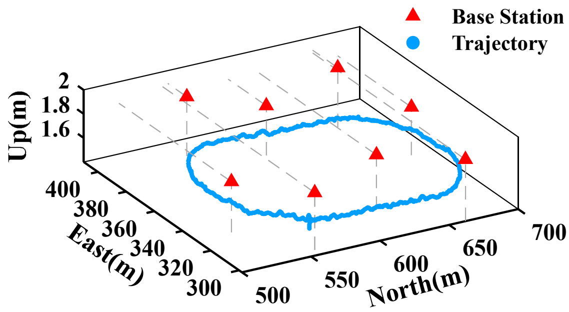

(**c**)

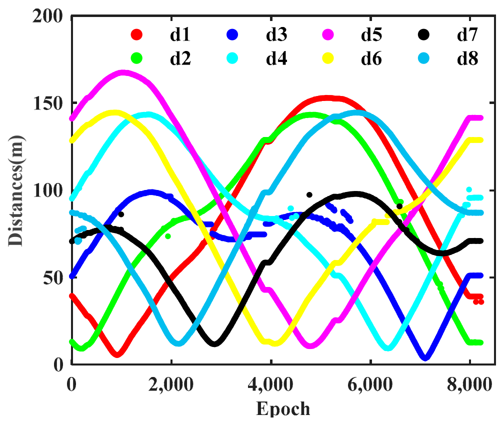

(**d**)

Figure 2. (**a**) Part of the used equipment; (**b**) the trajectory of the field test; (**c**) UWB base station distribution; (**d**) time-series of observed distances.

Table 2. Specification parameters of devices (https://www.nooploop.com/en/, accessed on 9 May 2023).

Parameters	LinkTrack P
Size	60.3 × 29 × 9 mm
Weight	33.3 g
Maximum Communication Distance	500 m
Recommended Distance	300 m
Maximum Sampling Rate	200 Hz
Recommended Sampling Rate	20 Hz
One, two-dimensional Accuracy	10 cm
Three-dimensional Accuracy	30 cm
Frequencies	4/4.5 GHz
Band-wide	499.2 MHz

3.1. Data Quality Analysis

The residuals of UWB data calculated by different algorithms based on both simulation experiments and measured experiments were presented in Figure 3. It can be seen that the residual distributions for the simulation data basically obeyed the normal distribution. For the measured data, they were significantly nonnormal distributions. This appearance was mainly caused by the NLOS error. However, the residual distributions of PF and RPF were closer to normal distribution. According to the statistics in Tables 3 and 4, the residuals indexes for LS, EKF, UKF, CKF, PF, and RPF were close to each other and a little better than Bancroft in simulation test in terms of average, STD, and Maximum. Such appearance can also be found in the field test. The difference in visible was that these three indexes in the field test were much bigger than those in the simulation test. It can be concluded that the conventional adjustment methods and the presented method had similar distribution characters, while the UWB data only contained Gauss noise. However, these adjustments will result in residual with obvious differences while suffering NLOS noise.

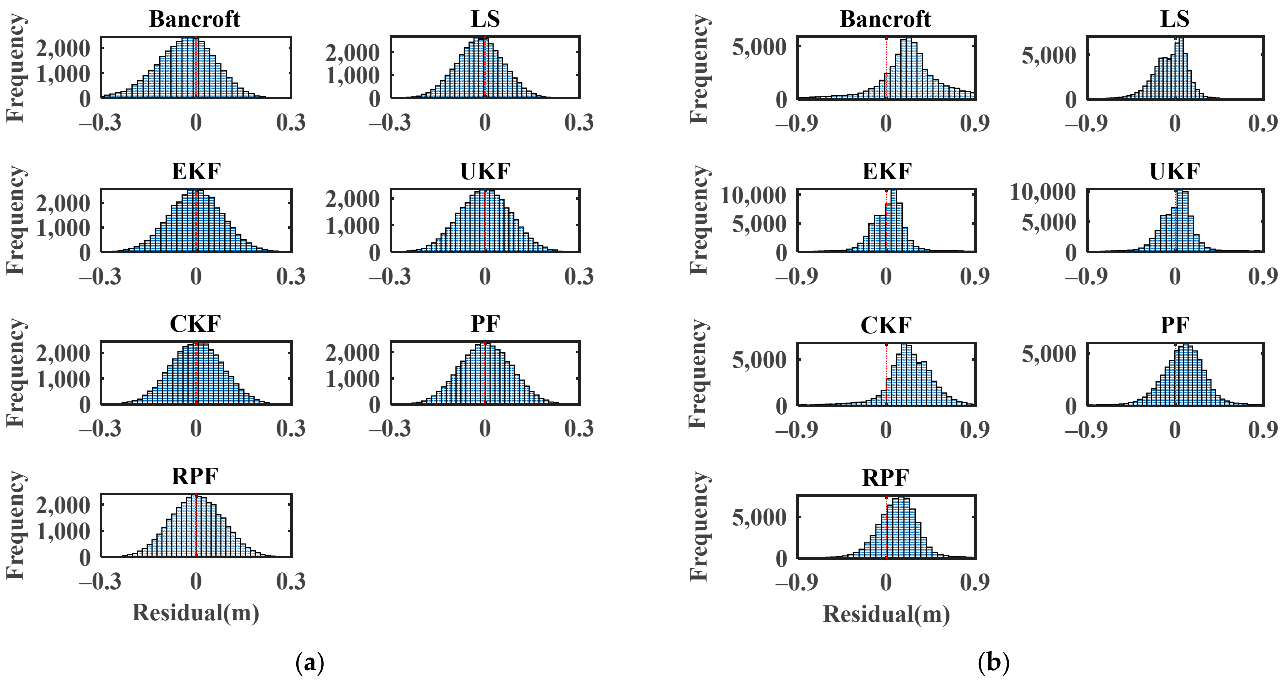

Figure 3. Residual histogram of UWB data in the simulation experiment (**a**) and these in the field experiment (**b**).

Table 3. Average, STD, and maximum values of residuals in the simulation experiment.

	Bancroft	LS	EKF	UKF	CKF	PF	RPF
Average (m)	−0.03	−0.02	−0.0008	0.0005	0.002	0.001	0.002
STD (m)	0.09	0.07	0.08	0.08	0.08	0.08	0.08
Max (m)	0.56	0.33	0.34	0.30	0.32	0.30	0.30

Table 4. Average, STD, and maximum values of residuals in the field experiment.

	Bancroft	LS	EKF	UKF	CKF	PF	RPF
Average (m)	0.25	−0.05	0.007	0.004	0.15	0.07	0.10
STD (m)	1.33	0.76	0.66	0.66	0.87	0.68	0.67
Max (m)	19.25	14.56	12.77	12.73	15.23	13.28	12.96

3.2. Evaluations Based on the Simulation Test

Figures 4 and 5 show the position error in horizontal and vertical in terms of scatter diagrams and time series, which were calculated by the seven adjustment algorithms (Bancroft, LS, EKF, UKC, CKF, PF, and RPF) based on the simulated UWB data. It can be seen that the position errors of the seven algorithms in horizontal (centimeter level) were much lower than those in vertical direction (meter level). This was majorly caused by the geometry distribution between eight base stations and tag. As shown in Figure 6, the HDOP values (0.73 on average) were much smaller than the corresponding VDOP (184.05 on average). Additionally, since only Gaussian noises and no NLOS errors were added in these simulated data, the position differences presented in the results can reflect the real performance of different adjustment methods directly. Accordingly, the Bancroft algorithm had the worst solutions because it solved the results of nonlinear system in non-optimal in the statistical properties. The results from the other algorithms were higher accuracy. Because the criteria of minimizing the squared observation-residuals and minimizing the squared parameter-residuals [46] were used to find the optimal solutions. Meanwhile, the position errors caused by linearization errors in both LS and EKF can be eliminated while using the UKF, CKF, and PF. Additionally, since only Gaussian noises and no NLOS errors were added in these simulated data, the robust algorithm in Equation (16) could not be activated. Therefore, it can be seen that no more position improvements can be obtained while using the RPF compared to that of PF.

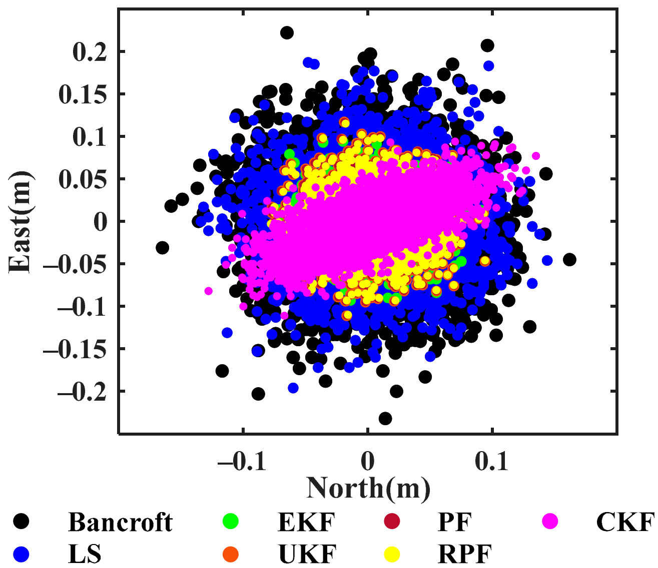

Figure 4. Horizontal position error in simulation test.

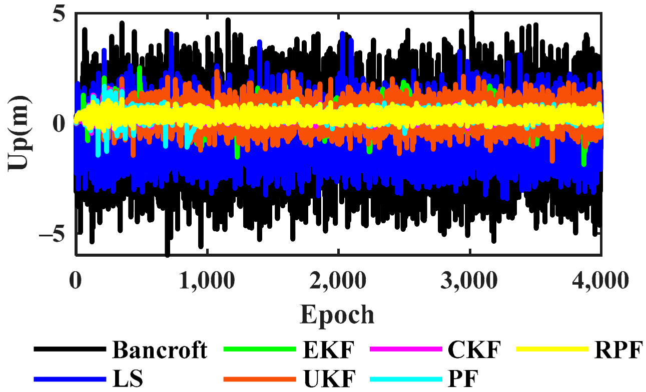

Figure 5. Time-series of vertical position errors in simulation test.

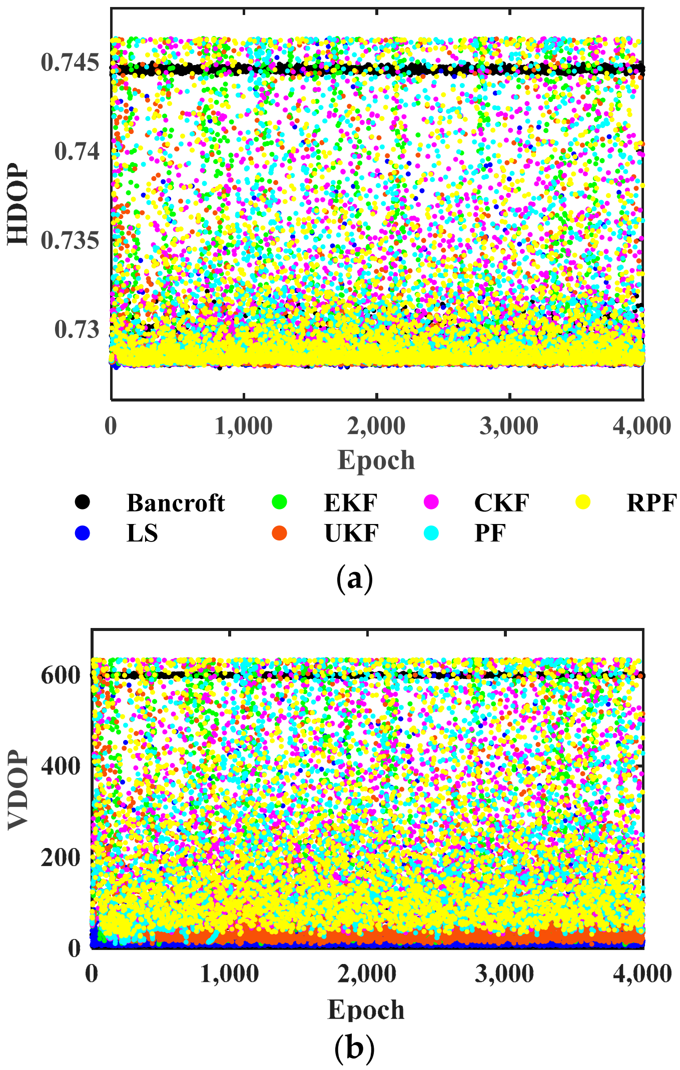

Figure 6. HDOP (**a**) and VDOP (**b**) of the simulation experiment.

Figure 7 shows the cumulative distribution function (CDF) of position errors of the seven positioning algorithms. It can be seen that the CDF of RPF, PF, and CKF have the highest probability in three-dimensional positioning error under the same threshold value. According to the CDF values of the localization error in Figure 7, at the percentage of 50%, 3D position errors for the Bancroft, LS, EKF, UKF, CKF, PF, and RPF were less than 0.43 m, 0.85 m, 0.42 m, 0.42 m, 0.37 m, 0.36 m, and 0.35 m, respectively. These values on the percentage of 68% for the Bancroft, LS, EKF, UKF, CKF, PF, and RPF were 2.07 m, 1.32 m, 0.65 m, 0.62 m, 0.45 m, 0.44 m, and 0.43 m, respectively. While setting the percentage to 95%, the 3D position errors for the seven algorithms were 3.77 m, 2.43 m, 1.32 m, 1.25 m, 0.69 m, 0.71 m, and 0.67 m. Since only Gaussian noises were added in these simulated UWB distances, it indicates that the truncation errors would degrade UWB position accuracy significantly, with a percentage of 13.6%, 16.3%, and 40.3% in the north, east, and vertical directions on average.

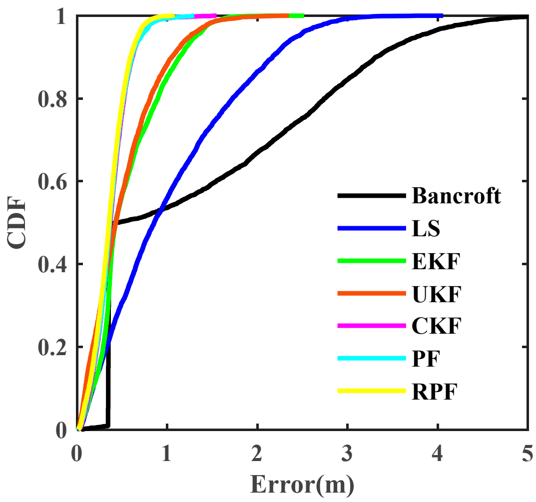

Figure 7. CDF of the 3D localization error.

Figure 8 shows the statistical results of position errors in terms of RMSE and average error. Comparing the horizontal positioning error in Figure 8b with the three-dimensional positioning error in Figure 8a, it can be seen that the RMSE of UWB positioning accuracy in horizontal was about 0.03 m~0.08 m, which was much higher than that in the vertical direction (0.36 m~1.91 m). Here, the 3D positioning RMSE of Bancroft, LS, EKF, UKF, CKF, PF, and RPF were 1.91 m, 1.28 m, 0.68 m, 0.64 m, 0.42 m, 0.41 m, and 0.40 m, respectively. Statistically, the RPF produced position accuracy improvements with percentages of 79.1%, 68.8%, 41.2%, 37.5%, 4.7%, and 2.4% to the solutions of Bancroft, LS, EKF, UKF, CKF, and PF, respectively. Additionally, the nonlinearization filters including UKF, CKF, PF, and RPF performed much higher accuracy than EKF and LS. It was because the nonlinear UWB positioning system needs to be linearized by using Taylor expansion which lead to the second-order and higher-order items being ignored. Such truncation errors could reduce positioning accuracy.

Table 5 lists the running time of the seven algorithms to complete the data processing. In general, the running time for the linearization estimation methods such as LS and EKF was much shorter than these of the nonlinearization filters (i.e., UKF, CKF, PF, and RPF). Even for the same type of estimation methods, the running times were also different. For example, the running times of LS and EKF were different. This was because a time-update phase was needed in EKF. Meanwhile, the CKF algorithm presented higher execution efficiency and less running time than the other nonlinearization filters, which was due to the fewer iterations. In general, RPF costs more running time, with about 16.4 times, 20.5 times, 6.5 times, 2.3 times, 3.6 times, and 1.3 times than that of Bancroft, LS, EKF, UKF, CKF, and PF, respectively.

Table 5. Algorithm running times in static simulation experiment.

	Bancroft	LS	EKF	UKF	CKF	PF	RPF
Time (s)	1.5	1.2	3.8	10.7	6.8	19.3	24.6

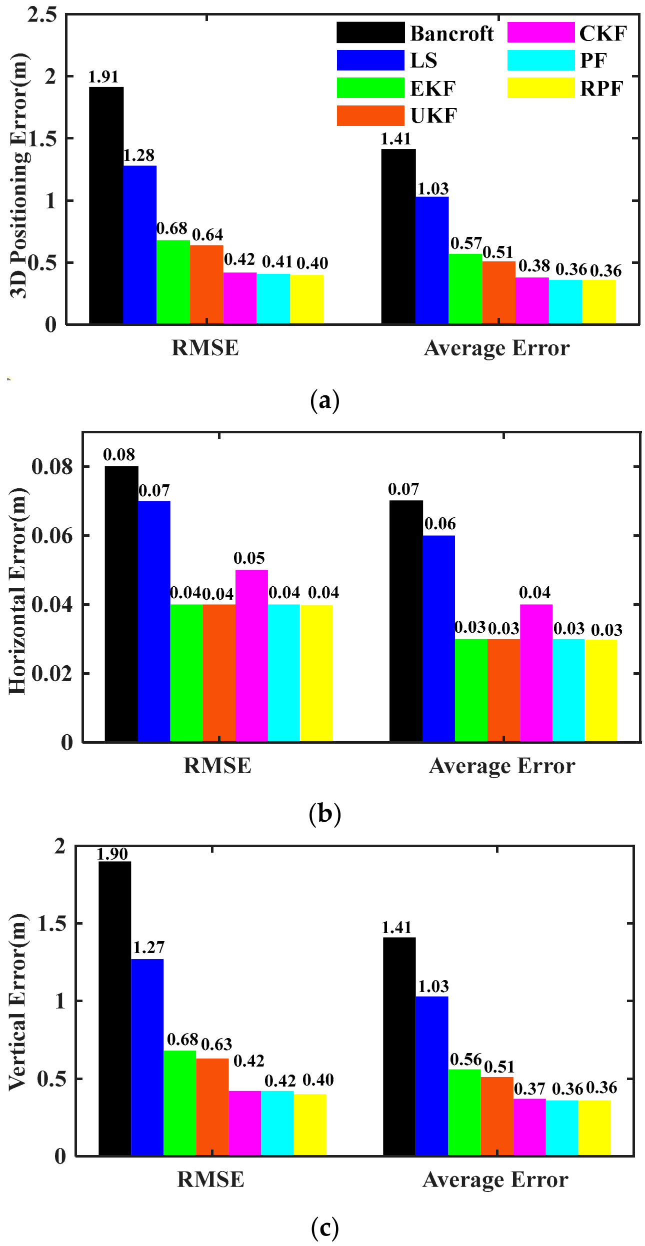

Figure 8. Positioning error statistics of different algorithms in static simulation experiments: (**a**) 3D positioning error statistics of different algorithms; (**b**) horizontal positioning error statistics of different algorithms; (**c**) vertical positioning error statistics of different algorithms.

3.3. Evaluations Based on the Field Test

Shown in Figure 9 are the positioning errors based on the practical UWB data. Compared with the simulation results, the positioning accuracies of all these positioning methods in practice were significantly degraded in both horizontal and vertical components. Such accuracy degradations were due to the coupled errors of NLOS, nonlinear error, and random noise. However, it can be seen that RPF can hold on the positioning accuracy compared to the other algorithms, while UWB distance suffered NLOS errors (i.e., around epochs 200–300, 3800–4000, and 6400–6600). In general, it benefitted from the resistance mechanism of RPF in Equation (16). In the vertical direction, the positioning errors of the LS algorithm were large. This was mainly because the differences in vertical of all the eight base stations were small, which lead to the inverse of $\boldsymbol{A}^{\mathrm{T}}\boldsymbol{A}$ being large and unstable. Additionally, the position errors in the vertical direction were much larger than those in the north and east directions. The main reason was that the geometry structure in the horizontal was much more reasonable than that in the vertical direction, which can be found in Figure 10. As is shown, the HDOP and VDOP were 0.79 and 77.35 on average. All of these reasons resulted in lower positioning accuracies in practical UWB tests. According to the CDF of the localization error in Figure 11, 95% of 3D position errors of the Bancroft, LS, EKF, UKF, CKF, PF, and RPF were less than 8.90 m, 4.95 m, 4.15 m, 4.05 m, 3.31 m, 3.89 m, and 2.91 m, respectively.

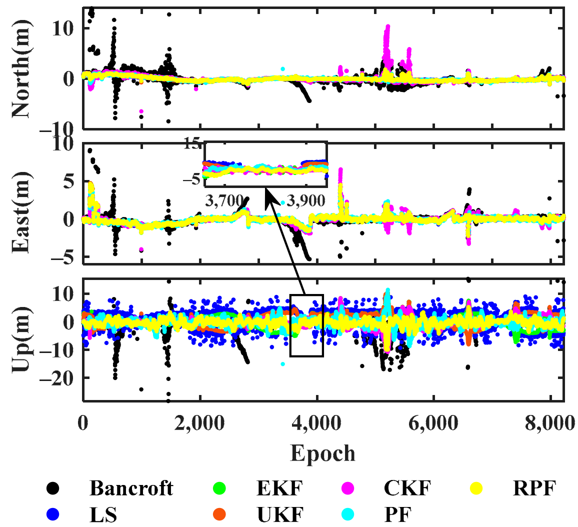

Figure 9. Time-series of positioning error in the field experiment.

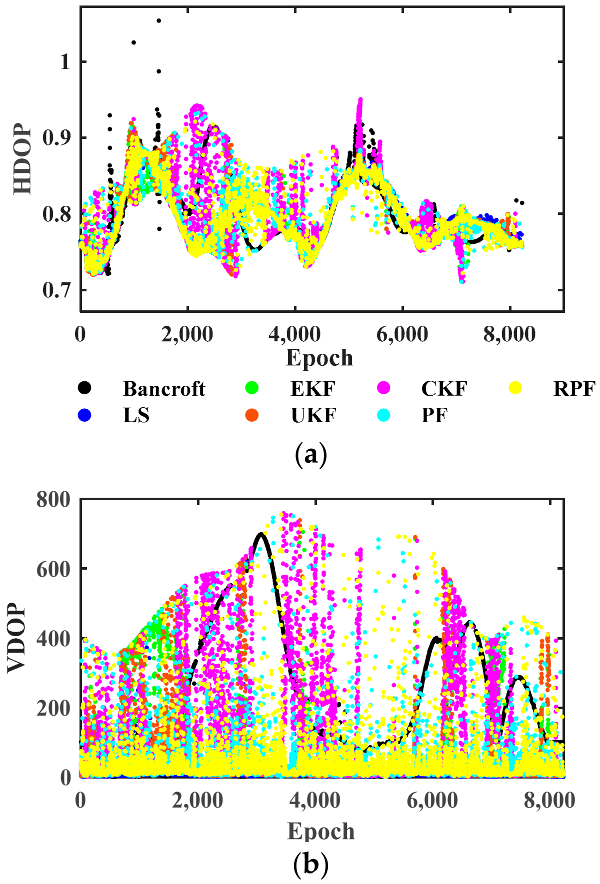

Figure 10. HDOP (**a**) and (**b**) VDOP in the field experiment.

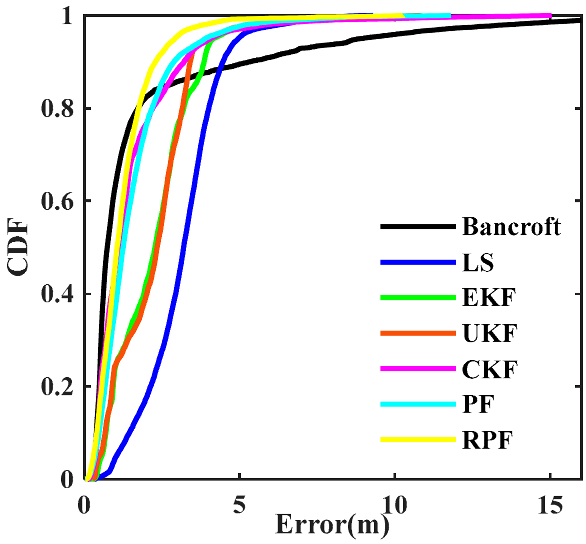

Figure 11. CDF of 3D positioning error in the field experiment.

Figure 12 shows the statistical results of UWB position errors in horizontal and vertical components of the seven algorithms in terms of RMSE and average errors, respectively. Similar to the simulation results, the horizontal positioning accuracy was much higher than the vertical positioning accuracy. Meanwhile, solutions from UKF and CKF were more accurate than that of EKF. This was because UKF and CKF acted as definite sampling filtering algorithms. While dealing with nonlinear system, sigma point sets were generated according to the sampling strategy based on the mean and covariance of the system state prior probability density. Therefore, it did not need to linearize UWB observation equations leading to no linearization errors. Meanwhile, the Jacobi matrices will not be needed during filtering algorithm iteration. However, the principle of avoiding linearization for UKF and CKF is different. For UKF, it is realized by computing the approximation term of the probability statistical eigenvalues of the nonlinear equation instead of ignoring the higher order term of the nonlinear equation after Taylor expansion [47]. The CKF is based on the theory of numerical integration and approximates the Gaussian integral by using the third-order spherical radial volume criterion [48]. Therefore, CKF is more rigorous and stable than UKF in theory. The statistical results in Figure 12 prove it visibly. For the least square method, it avoids the explicit inversion of the matrix, and guarantees the symmetry and positivity of the covariance matrix. It can be seen from Figure 12a that the 3D positioning RMSE values of Bancroft, LS, EKF, UKF, CKF, PF, and RPF were 2.86 m, 3.38 m, 2.51 m, 2.45 m, 1.89 m, 1.85 m, and 1.41 m, respectively. Compared with the solutions of Bancroft, LS, EKF, UKF, CKF, and PF, RPF upgraded the position accuracy by 50.7%, 58.3%, 43.8%, 42.4%, 25.4%, and 23.8%, respectively. This indicates that the truncation errors would degrade UWB position accuracy significantly, with the percentages of 2.5%, 3.9%, and 26.1% in the north, east, and vertical components on average. Such accuracy-decrease rates caused by NLOS error were 6.1%, 5.2%, and 25.1% in the three directions. Therefore, when UWB ranging distance contained NLOS errors, the robust algorithm in RPF can remove the impact of NLOS on UWB position accuracy. Table 6 lists the running times required for the seven algorithms. It can be seen that the RPF algorithm took the most time, which was about 18.4 times, 8.9 times, 8.2 times, 2.3 times, 3.8 times, and 1.1 times more than that of Bancroft, LS, EKF, UKF, CKF, and PF, respectively. This conclusion is consistent with the results from the simulation experiment.

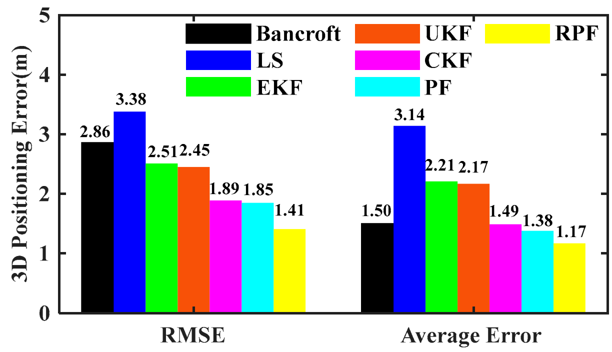

(**a**)

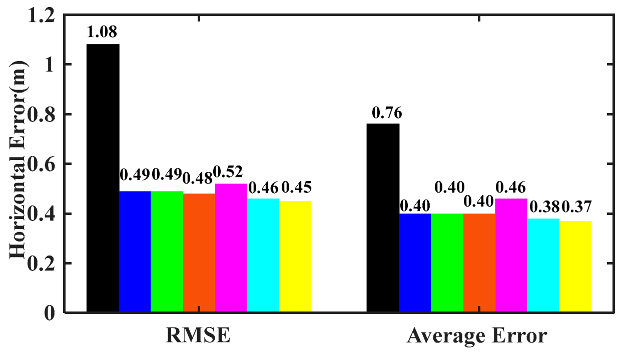

(**b**)

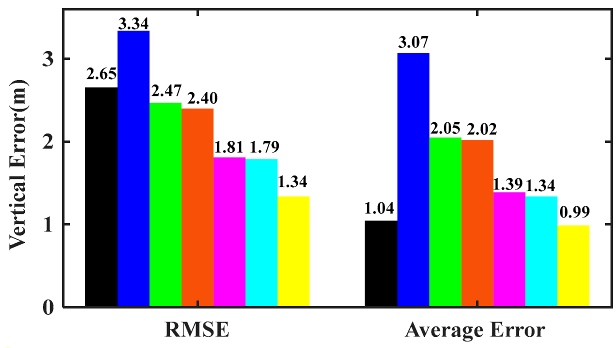

(**c**)

Figure 12. Positioning error statistics of different algorithms in the field experiment: (**a**) 3D positioning error statistics of different algorithms; (**b**) horizontal positioning error statistics of different algorithms; (**c**) vertical positioning error statistics of different algorithms.

Table 6. Algorithm running times in field experiment.

	Bancroft	LS	EKF	UKF	CKF	PF	RPF
Time (s)	2.8	5.8	6.3	21.9	13.6	45.4	51.6

4. Conclusions

Aiming at evaluating the impacts of linearization errors and NLOS errors on UWB positioning accuracy, a robust particle filter UWB positioning algorithm based on IGGIII was presented in this paper. Meanwhile, traditional UWB positioning methods such as Bancroft, LS, EKF, UKF, CKF, and PF were used to aid separating the independent influences of such two kinds of errors on the UWB positioning performance. The results based on TOF-UWB data in the simulation test and field test demonstrated that (1) the linearization errors exist in UWB positioning significantly while using linearization adjustments (i.e., LS and EKF). However, it can be eliminated by using the nonlinearized filter (i.e., UKF, CKF, and

PF). Such elimination would be weakened by the coupled errors in UWB measurements. When there was only white noise (as shown in the simulation test), the nonlinearized filters provided visible accuracy improvements. Otherwise, the improvements will be invisible while coupling with a strong NLOS signal. (2) The IGGIII robust algorithm can constrain the impact of NLOS errors on UWB positioning accuracy obviously. In general, compared to the solutions from the Bancroft, LS, EKF, UKF, CKF, and PF, the RPF produced 64.9%, 63.5%, 42.5%, 39.9%, 15.1%, and 13.1% 3D position improvements on average, respectively. The truncation errors and NLOS errors can, respectively, lead to 36.6% and 23.7% accuracy degradations in UWB 3D positioning. However, the presented method cost more running time than the other methods, with about 17.4 times, 14.7 times, 7.3 times, 2.3 times, 3.7 times, and 1.2 times compared to the times needed in Bancroft, LS, EKF, UKF, CKF, and PF. In addition, the horizontal accuracy of UWB (centimeter level) was much higher than those in the vertical direction (meter level) own to the geometry structure between the tag and base stations. Based on the conclusions in this paper, the goal in our future work is to upgrade the UWB positioning accuracy in the vertical component.

Author Contributions: Data curation, Y.L. and Q.X.; funding acquisition, Z.G.; investigation, Q.X.; methodology, Y.L. and Z.G.; software, Y.L.; supervision, C.Y.; validation, Y.L.; visualization, Y.L.; writing—original draft, Y.L.; writing—review and editing, Z.G. and C.Y. All authors have read and agreed to the published version of the manuscript.

Funding: This work was partially funded by the National Key Research and Development Program of China (Grant No. 2021YFB3901301), the National Natural Science Foundation of China (NSFC) (Grants No. 42274022).

Institutional Review Board Statement: Not applicable.

Informed Consent Statement: Not applicable.

Data Availability Statement: The datasets adopted in this paper can be available on request from the corresponding author.

Conflicts of Interest: The authors declare no conflict of interest.

References

1. Jiang, C.H.; Shen, J.C.; Chen, S.; Chen, Y.W.; Liu, D.; Bo, Y.M. UWB NLOS/LOS Classification Using Deep Learning Method. *IEEE Commun. Lett.* **2020**, *24*, 2226–2230. [CrossRef]
2. Xu, Y.; Ahn, C.K.; Shmaliy, Y.S.; Chen, X.; Bu, L. Indoor INS/UWB-based Human Localization With Missing Data Utilizing Predictive UFIR Filtering. *IEEE-CAA J. Autom. Sin.* **2019**, *6*, 952–960. [CrossRef]
3. Magsino, E.R.; Ho, I.W.-H.; Situ, Z. The Effects of Dynamic Environment on Channel Frequency Response-based Indoor Positioning. In Proceedings of the 28th Annual IEEE International Symposium on Personal, Indoor, and Mobile Radio Communications (PIMRC), Montreal, QC, Canada, 8–13 October 2017.
4. Tariq, O.B.; Lazarescu, M.T.; Lavagno, L. Neural networks for indoor person tracking with infrared sensors. *IEEE Sens. Lett.* **2021**, *5*, 6000204. [CrossRef]
5. Haigh, S.; Kulon, J.; Partlow, A.; Rogers, P.; Gibson, C. A Robust Algorithm for Classification and Rejection of NLOS Signals in Narrowband Ultrasonic Localization Systems. *IEEE Trans. Instrum. Meas.* **2019**, *68*, 646–655. [CrossRef]
6. Zhuang, Y.; Yang, J.; Li, Y.; Qi, L.; El-Sheimy, N. Smartphone-Based Indoor Localization with Bluetooth Low Energy Beacons. *Sensors* **2016**, *16*, 596. [CrossRef] [PubMed]
7. Shi, Y.; Zhang, W.; Yao, Z.; Li, M.; Liang, Z.; Cao, Z.; Zhang, H.; Huang, Q. Design of a Hybrid Indoor Location System Based on Multi-Sensor Fusion for Robot Navigation. *Sensors* **2018**, *18*, 3581. [CrossRef] [PubMed]
8. Magsino, E.; Barrameda, J.M.C.; Puno, A.; Ong, S.; Siapco, C.; Vibal, J. Determining Commercial Parking Vacancies Employing Multiple WiFiRSSI Fingerprinting Method. *J. Sens. Actuator Netw.* **2023**, *12*, 22. [CrossRef]
9. Khalili, B.; Ali Abbaspour, R.; Chehreghan, A.; Vesali, N. A Context-Aware Smartphone-Based 3D Indoor Positioning Using Pedestrian Dead Reckoning. *Sensors* **2022**, *22*, 9968. [CrossRef]
10. Zhang, L.; Huang, L.; Yi, Q.; Wang, X.; Zhang, D.; Zhang, G. Positioning Method of Pedestrian Dead Reckoning Based on Human Activity Recognition Assistance. In Proceedings of the 12th IEEE International Conference on Indoor Positioning and Indoor Navigation (IPIN), Beijing, China, 5–7 September 2022.
11. Shang, S.; Wang, L. Overview of WiFi fingerprinting-based indoor positioning. *IET Commun.* **2022**, *16*, 725–733. [CrossRef]
12. Nguyen, D.T.A.; Joung, J.; Kang, X. Deep Gated Recurrent Unit-Based 3D Localization for UWB Systems. *IEEE Access* **2021**, *9*, 68798–68813. [CrossRef]

13. Liu, Y. UWB ranging error analysis based on TOA mode. In *Proceedings of Journal of Physics: Conference Series*; IOP Publishing: Bristol, UK, 2021; p. 012124.
14. Otim, T.; Bahillo, A.; Diez, L.E.; Lopez-Iturri, P.; Falcone, F. Towards Sub-Meter Level UWB Indoor Localization Using Body Wearable Sensors. *IEEE Access* **2020**, *8*, 178886–178899. [CrossRef]
15. Albaidhani, A.; Morell, A.; Vicario, J.L. Anchor selection for UWB indoor positioning. *Trans. Emerg. Telecommun. Technol.* **2019**, *30*, e3598. [CrossRef]
16. Zhao, Y.; Zou, J.; Guo, J.; Huang, G.; Cai, L. A Novel Ultra-Wideband Double Difference Indoor Positioning Method with Additional Baseline Constraint. *ISPRS Int. J. Geo-Inf.* **2021**, *10*, 634. [CrossRef]
17. Huang, Z.; Jin, S.; Su, K.; Tang, X. Multi-GNSS Precise Point Positioning with UWB Tightly Coupled Integration. *Sensors* **2022**, *22*, 2232. [CrossRef]
18. Li, M.-G.; Zhu, H.; You, S.-Z.; Tang, C.-Q. UWB-Based Localization System Aided With Inertial Sensor for Underground Coal Mine Applications. *IEEE Sens. J.* **2020**, *20*, 6652–6669. [CrossRef]
19. Djosic, S.; Stojanovic, I.; Jovanovic, M.; Nikolic, T.; Djordjevic, G.L. Fingerprinting-assisted UWB-based localization technique for complex indoor environments. *Expert Syst. Appl.* **2021**, *167*, 114188. [CrossRef]
20. Han, Y.; Zhang, X.; Lai, Z.; Geng, Y. TOF-Based Fast Self-Positioning Algorithm for UWB Mobile Base Stations. *Sensors* **2021**, *21*, 6359. [CrossRef] [PubMed]
21. Tian, K.; Radovnikovich, M.; Cheok, K. Comparing EKF, UKF, and PF Performance for Autonomous Vehicle Multi-Sensor Fusion and Tracking in Highway Scenario. In Proceedings of the 16th Annual IEEE International Systems Conference (SysCon), Electr Network, Virtual, 25 April–23 May 2022.
22. Guvenc, I.; Chong, C.-C.; Watanabe, F. NLOS identification and mitigation for UWB localization systems. In Proceedings of the 2007 IEEE Wireless Communications and Networking Conference, Washington, DC, USA, 1–15 March 2007; pp. 1571–1576.
23. Li, S.; Li, G.; Wang, L.; Zhou, Y.; Peng, Y.; Fu, J. A three-dimensional robust ridge estimation positioning method for UWB in a complex environment. *Adv. Space Res.* **2017**, *60*, 2763–2775. [CrossRef]
24. Dong, J.; Lian, Z.; Xu, J.; Yue, Z. UWB Localization Based on Improved Robust Adaptive Cubature Kalman Filter. *Sensors* **2023**, *23*, 2669. [CrossRef]
25. Fu, J.; Fu, Y.; Xu, D. Application of an Adaptive UKF in UWB Indoor Positioning. In Proceedings of the Chinese Automation Congress (CAC), Hangzhou, China, 22–24 November 2019; pp. 544–549.
26. Wu, Q.; Liu, Z.; Zhang, J.; Sun, K. Ultra-Wideband-based Trajectory Estimation Algorithm with Adaptive Square Root Cubature Kalman Filtering. *J. Eng. Sci. Technol. Rev.* **2016**, *9*, 140–147.
27. Tang, C.; Zhou, D.; Dou, L.; Jiang, C. A 3D Range-Only SLAM Algorithm Based on Improved Derivative UKF. *Electronics* **2022**, *11*, 1109. [CrossRef]
28. Poulose, A.; Han, D.S. UWB Indoor Localization Using Deep Learning LSTM Networks. *Appl. Sci.* **2020**, *10*, 6290. [CrossRef]
29. Zhang, H.; Ayoub, R.; Sundaram, S. Sensor selection for Kalman filtering of linear dynamical systems: Complexity, limitations and greedy algorithms. *Automatica* **2017**, *78*, 202–210. [CrossRef]
30. Cho, S.Y. CKF-based Fast Error Compensation Filter Design for IR-UWB Indoor Positioning System for Building Automation. In Proceedings of the 2018 IEEE 14th International Conference on Automation Science and Engineering (CASE), Munich, Germany, 20–24 August 2018; pp. 668–670.
31. Axel, B.; Silvere, B. The Invariant Extended Kalman Filter as a Stable Observer. *IEEE Trans. Autom. Control* **2017**, *62*, 1797–1812.
32. Ma, F.; He, J.; Zhang, X. Robust Kalman Filter Algorithm Based on Generalized Correntropy for Ultra-Wideband Ranging in Industrial Environment. *IEEE Access* **2019**, *7*, 27490–27500. [CrossRef]
33. Han, H.; Wang, J.; Liu, F.; Zhang, J.; Yang, D.; Li, B. An Emergency Seamless Positioning Technique Based on ad hoc UWB Networking Using Robust EKF. *Sensors* **2019**, *19*, 3135. [CrossRef] [PubMed]
34. Zhang, J.; Wang, J.; Cui, X.; Yuan, D. BDS/GPS/UWB Adaptively Robust EKF Tightly Coupled Navigation Model Considering Pedestrian Motion Characteristics. *Remote Sens.* **2022**, *14*, 1940. [CrossRef]
35. Chen, Z.; Xu, A.; Sui, X.; Wang, C.; Wang, S.; Gao, J.; Shi, Z. Improved-UWB/LiDAR-SLAM Tightly Coupled Positioning System with NLOS Identification Using a LiDAR Point Cloud in GNSS-Denied Environments. *Remote Sens.* **2022**, *14*, 1380. [CrossRef]
36. Cheng, L.; Zhang, H.; Wei, D.; Zhou, J. An Indoor Tracking Algorithm Based on Particle Filter and Nearest Neighbor Data Fusion for Wireless Sensor Networks. *Remote Sens.* **2022**, *14*, 5791. [CrossRef]
37. Tian, Q.; Wang, K.I.K.; Salcic, Z. A Resetting Approach for INS and UWB Sensor Fusion Using Particle Filter for Pedestrian Tracking. *IEEE Trans. Instrum. Meas.* **2020**, *69*, 5914–5921. [CrossRef]
38. Li, Z.; Wu, J.; Kuang, Z.; Zhang, Z.; Zhang, S.; Dong, L.; Zhang, L. Moving Target Tracking Algorithm Based on Improved Resampling Particle Filter in UWB Environment. *Wirel. Commun. Mob. Comput.* **2022**, *2022*, 9974049. [CrossRef]
39. Zhou, M.; Wang, B.; Tian, Z.; Xie, L. Hardware and software design of BMW system for multi-floor localization. *EURASIP J. Wirel. Commun. Netw.* **2017**, *2017*, 139. [CrossRef]
40. Espes, D.; Maria Pistea, A.; Canaff, C.; Iordache, I.; Le Parc, P.; Radoi, E. New Method for Localization and Human Being Detection using UWB Technology: Helpful Solution for Rescue Robots. In Proceedings of the 3rd Workshop on Robots and Sensors Integration in Future Rescue Information System (ROSIN'13), Tokyo, Japan, 7 November 2013; p. 6.
41. Yu, H.; Huang, G.; Gao, J.; Liu, B. An Efficient Constrained Weighted Least Squares Algorithm for Moving Source Location Using TDOA and FDOA Measurements. *IEEE Trans. Wirel. Commun.* **2012**, *11*, 44–47. [CrossRef]

42. You, W.; Li, F.; Liao, L.; Huang, M. Data Fusion of UWB and IMU Based on Unscented Kalman Filter for Indoor Localization of Quadrotor UAV. *IEEE Access* **2020**, *8*, 64971–64981. [CrossRef]
43. Li, Z.; Zhang, L.; Tian, G. UWB/PDR integrated indoor positioning method based on robust adaptive square root cubature Kalman filter. In *Proceedings of Journal of Physics: Conference Series*; IOP Publishing: Bristol, UK, 2021; p. 012021.
44. Zhang, X.; Kuang, Y.; Yang, H.; Lu, H.; Yang, Y. UWB Indoor Localization Algorithm Using Firefly of Multistage Optimization on Particle Filter. *J. Sens.* **2021**, *2021*, 1383767. [CrossRef]
45. Huber, P.J.J.A.o.M.S. Robust Estimation of a Location Parameter. *Breakthr. Stat. Methodol. Distrib.* **1964**, *35*, 492–518. [CrossRef]
46. Yang, Y. *Adaptive Navigation and Kinematic Positioning*; Surveying and Mapping Press: Beijing, China, 2006.
47. Julier, S.J.; Uhlmann, J. Unscented filtering and nonlinear estimation. *Proc. IEEE* **2004**, *92*, 401–422. [CrossRef]
48. Arasaratnam, I.; Haykin, S. Cubature kalman filters. *IEEE Trans. Autom. Control* **2009**, *54*, 1254–1269. [CrossRef]